ISSN 1990-7931, Russian Journal of Physical Chemistry B, 2019, Vol. 13, No. 1, pp. 49–61. © Pleiades Publishing, Ltd., 2019.

KINETICS AND MECHANISM OF CHEMICAL REACTIONS. CATALYSIS

Synthesis, Characterization, Computation of Global Reactivity Descriptors and Antiproliferative Activity of *N*-(4-nitrophenyl)Acrylamide[1]

Emine Tanış[a], *, Nevin Çankaya[b], and Serap Yalçın[c]

[a] *Health Services Vocational School, Kırşehir Ahi Evran University, Kırşehir, Turkey*

[b] *Department of Chemistry, Usak University, Uşak, Turkey*

[c] *Department of Molecular Biology and Genetic, Kırşehir Ahi Evran University, Kırşehir, Turkey*

**e-mail: eminetanis@ahievran.edu.tr*

Received March 19, 2018; revised June 19, 2018; accepted August 20, 2018

Abstract—In this article *N*-(4-nitrophenyl)acrylamide has been synthesized and characterized both experimentally and theoretically. The synthesized monomer was characterized experimentally by Fourier Transform Infrared, Nuclear Magnetic Resonance spectroscopic techniques and theoretically by Density Functional Theory and Time-Dependent Density Functional Theory methods at Coulomb Attenuated Method level. To investigate the natural toxicity and reactivity of the title molecule optimized at the Density Functional Theory/ Coulomb Attenuated Method- Becke three-parameter Lee–Yang–Parr level, the chemical reactivity descriptors were calculated based on the rotational barriers. Using the Parr formula, the interaction between *N*-(4-nitrophenyl)acrylamide molecule and nucleic acid bases (adenine, thymine, cytosine, uracil and guanine) phenylalanine and histidine an Aryl Hydrocarbon hydroxylase receptors were investigated. Charge transfer that is important in the formation of chemically bonded adducts causing cancer has been calculated quantitatively. In addition, in vitro cytotoxicity of *N*-(4-nitrophenyl)acrylamide on HeLa cell lines has been studied. It has been found that the half maximal inhibitory concentration value of *N*-(4-nitrophenyl)acrylamide is 1 mM in HeLa cells. Our results show that *N*-(4-nitrophenyl)acrylamide, an acrylamide-based molecule that is accepted as toxic by the World Health Organization, has low toxicity on cancer cells by experimental study and, in theory, it has low toxicity according to calculations of reactivity descriptors, therefore can be used for biomedical research.

Keywords: *N*-(4-nitrophenyl)acrylamide (4NPA), density functional theory, time-dependent approach, HeLa cell line, antiproliferative activity

DOI: 10.1134/S1990793119010147

1. INTRODUCTION

Acrylamide is a common organic compound used in various products in either its monomeric or polymeric forms. Monomer acrylamide is reported as a neurotoxin agent according to the laboratory studies on animals and it is suspected to be carcinogenic to both animals and humans. Although monomeric acrylamide is considered to be more harmful than polymeric, polymeric acrylamide has also been reported to be dangerous when it contaminates food [1–4]. Acrylamide could be consumed by respiration, orally or dermally [5]. Effects of acrylamide on health could be classified as toxic and carcinogenic, which both come from its carcinogenic properties [6–9].

Acrylamide monomers consist of acryl and amide groups that contain vinyl group. Acrylamide is a compound with weak acidic property, has a white crystalline structure, and is odorless, soluble in solvents such as water, alcohol, ether and acetone while insoluble in heptane and benzene [1]. Markastokk et al., [10] have performed a number of quantum chemical calculations for acrylamide at Hartree–Fock (HF), Møller–Plesset perturbation theory (MP2) and Density Functional Theory (DFT) levels. Toxic substances exhibit behavior as electron acceptors during the charge transfer phase. This fact has been verified in previous studies [11–13]. Therefore, the electron affinity parameter can be used to understand the toxic effect of acrylamide and its derivatives.

Acrylamide based *N*-(4-nitrophenyl)acrylamide (4NPA) monomer which has been synthesized by us—and the subject of this study—is a compound which has a green crystalline structure, odorant, insoluble in solvents such as water, alcohol, ether and acetone, and soluble in solvents such as *N*,*N*-Dimethylformamide, Dimethyl sulfoxide. This property of the monomer

[1] The article is published in the original.

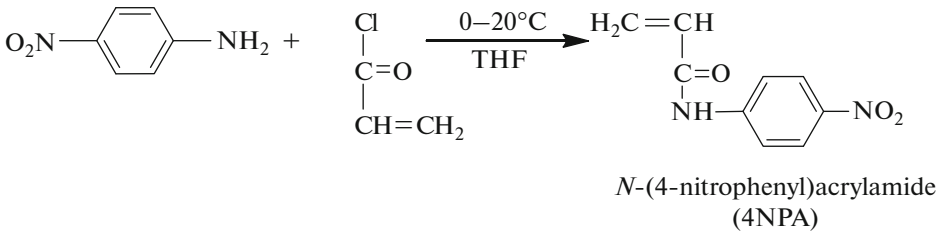

N-(4-nitrophenyl)acrylamide
(4NPA)

Fig. 1. The synthesis of 4NPA.

probably comes from the phenyl ring and NO_2 groups in its structure. The groups NO_2 and C_3H_5NO (acrylamide) bound to the phenyl ring can freely rotate around the single bond attached to the ring and thus form new molecules. Therefore, it is important to evaluate the single bond rotation potential in order to understand the structure and interaction of the organic molecules and their reactivity and toxicity.

Efforts to determine the toxic potential of various compounds, from small molecules to biosystems, are a large part of toxicity studies [14–16]. Biological experiments are often limited in terms of sample, time and cost. In this context, recent studies have shown that the DFT-based reactivity descriptors are advantageous and can be compared with the experimental observations [17]. The reactivity descriptors calculated using the DFT method play an important and reliable role in many studies [11–29]. Global hardness (η), electrophilicity index (ω), chemical potential (μ) and electronegativity (χ) are a few examples of these reactivity indicators. Global hardness is a measure of resistance to change in electron density. The chemical potential, which is negative for electronegativity ($\chi = -\mu$), is defined as the escape power of electrons from the molecule. The electrophilicity calculates a molecule's potential to accept an electron from the surrounding donor. Therefore, electrophilicity is an important parameter in determining toxicity. These descriptors were used to examine the toxicity of the molecules in previously conducted a few studies [17–21]. Schuurmann [30] used a combination of η and χ as identifiers with a lot of identifiers in the study of toxicities with Quantitative structure–activity relationship **(**QSAR) analysis for the 10 phophorothionates compound. Kobayashi et al. [31] showed that the relationship between chemical hardness of biological activities for selective dioxins. The various reactivity identifiers were calculated by the ''conceptional DFT'' method, which was then used by the Parr and Yang [32] proposed by Chermette [33]. Parthasarathi et al. [19, 34] analyzed the toxicity of two different molecules by means of chemical reactivity and selectivity profiles using DFT approach. In the above studies it appears that DFT calculations at higher theoretical levels are of importance in terms of being useful and less time-consuming to understand the toxicological activities of toxins. In addition, toxicity is thought to result from possible transfer of charge between a toxin and a biosystem [18, 34, 35]. Here, a model biosystem was constructed from selective nucleic acid bases (NA) and Aryl Hydrocarbon hydroxylase receptors (AHH), since a toxin is expected to interact with NA bases and AHH receptors.

In this study, the experimental and theoretical characterization, reactivity and toxicity of the newly synthesized 4NPA monomer were determined. To do this, the vibration numbers and chemical shifts are theoretically and experimentally determined and the experimental results were compared with the theoretical results calculated at the DFT/Coulomb Attenuated Method/Becke three-parameter Lee–Yang–Parr (CAM-B3LYP) 6-311++G(*d*,*p*) level. We have investigated DFT-based reactivity parameters depending on the torsional angle. For this purpose, the HOMO-LUMO energy values of the 4NPA molecule were first calculated. We calculated the amount of charge transfer between a model biosystem and a 4NPA molecule, which is thought to be toxic, to have information about toxic behavior in a biosystem using the highest occupied molecular orbital- lowest unoccupied molecular orbital (HOMO – LUMO) energy values. We chose NA bases (adenine, thymine, cytosine, uracil and guanine) and histidine and phenylalanine, AHH receptors, as a model biomolecules in this study. Furthermore, cytotoxicity measured in vitro on HeLa cell lines of 4NPA and calculated.

2. EXPERIMENTAL

Synthesis of N-(4-nitrophenyl)Acrylamide (4NPA)

Chemicals: *p*-Nitraniline, acrylic chloride and triethylamine [$(Et)_3N$] (Aldrich) were used as received. Tetrahydrofuran and chloroform as a solvent were dried on anhydrous $MgSO_4$. *p*-Nitraniline (1 mole) and $(Et)_3N$ (1 mole) dissolved in Tetrahydrofuran. Acrylic chloride (1.2 mole) was diluted in Tetrahydrofuran and, the reaction mixture was added dropwise to the solution with stirring at 0–5°C. It was then kept at room temperature with constant stirring for about 12 hours. The reaction mixture was precipitated in iced water and then, recrystallized in chloroform [36]. Synthesis of 4NPA monomer is shown in Fig. 1.

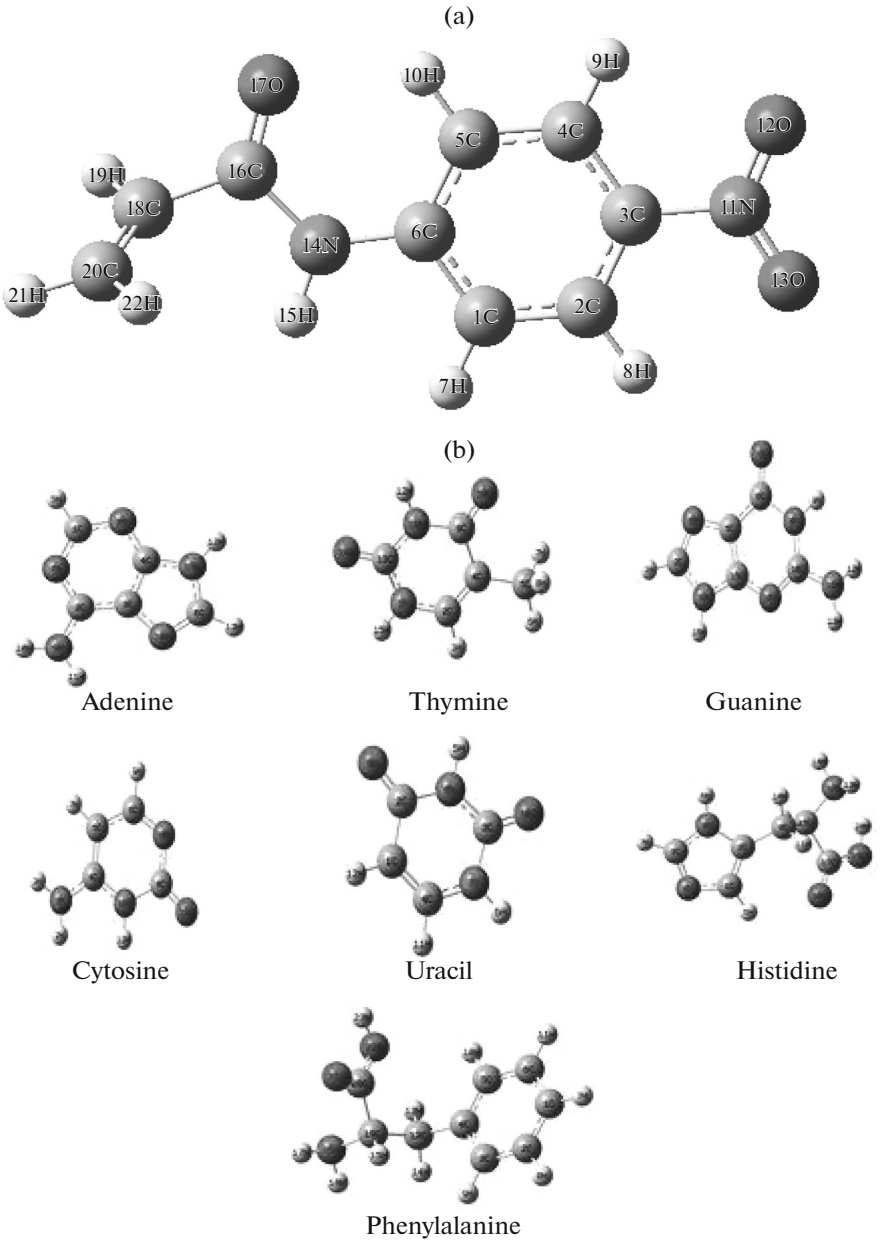

Fig. 2. (a) The optimized geometric structures of 4NPA; (b) The optimized geometry of the selected NA bases and AHH receptors.

3. METHODS AND MATERIALS

3.1. Theoretical Calculation

The optimized geometry of 4NPA is shown in Fig. 2a with the atom numbering. All quantum chemistry Density functional theory (DFT) calculations are carried out using GAUSSIAN 09 package [37]. The geometry of 4NPA is optimized by using a new hybrid exchange–correlation function named a Coulomb-attenuated hybrid exchange-correlation function (CAM-B3LYP), which includes both the hybrid qualities of B3LYP and the long-range correction presented by Tawada et al. [38]. Previous studies [39–41] on similar molecular systems with CAM-B3LYP in comparison because it provides reliable results, we used the same basic set in this study. The relative energy of 4NPA was calculated from 0° to 360° at 30° intervals as a function of the torsional angle φ (the rotation at the N14–C6 bond and the higher impact value of the conformation of the molecule seen to be the rotation through N14–C6). To calculate the relative energy, the geometry at various φ values are optimized at CAM-B3LYP/6–311++G(*d*,*p*) level. The relative energy for 4NPA is calculated as $\Delta E(\varphi) = [E(\varphi) - E(\varphi) = 180.0)]$ using the total energies of respective optimized conformations. Further the geometries for the model biomolecules are optimized using

6–311++G(*d*,*p*) basis set in the framework of CAM-B3LYP theory and presented in Fig. 2b. We have obtained the amount of charge transfer between headline molecule and model biomolecules.

Frontier molecular orbitals (HOMO and LUMO) are performed and analyzed. It is important to explain the reactivity of a chemical species, the most occupied molecular orbital named HOMO, and the least empty molecular orbital named LUMO. This was first recognized by Fukui [42]. There is a direct correlation between E_{HOMO} and toxicity. E_{HOMO} is often associated with the electron donor ability of the molecule. A molecule's high HOMO energy ensures that the appropriate receptor molecules have the potential to provide low energy electrons to the empty molecular orbital. Similarly E_{LUMO} is an indication of the ability of the molecule to accept electrons. The less valuable the E_{LUMO}, the more probable it is that the molecule would accept electrons. As a results, concerning the value of the energy of the gap $\Delta E = E_{LUMO} - E_{HOMO}$, larger values of the energy difference will provide low reactivity to a chemical reaction. The global hardness (η) has been indicated to be a very powerful tool global index of reactivity in atoms, molecules and clusters [43, 44]. The theoretical definition of chemical hardness has been provided by the DFT as the second derivative of electronic energy with respect to the number of electrons N, for a constant external potential $V(r)$:

$$\eta = 1/2\left(\partial^2 E/\partial N^2\right)_{V(r)} = 1/2\left(\frac{\partial \mu}{\partial N}\right)_{V(r)}, \quad (1)$$

where E is the total energy, N is the number of electrons of the chemical species and μ is the chemical potential, which is identified as the negative of the electronegativity χ as defined by Iczkowski and Margrave [45]. By applying finite difference approximation to Eq. (1) we get the operational definition for η as:

$$\eta = (IP - EA)/2. \quad (2)$$

Eq. (2) can be rewritten as follows using Koopmans' [43] theorem as:

$$\eta = (\varepsilon_{LUMO} - \varepsilon_{HOMO})/2. \quad (3)$$

Parr et al. [46] introduced the global electrophilicity index (μ) in relation to chemical potential and hardness as:

$$\omega = \mu^2/2\eta. \quad (4)$$

For the possible toxicity of the 4NPA, the various reactivity and descriptors such as chemical hardness (η) calculated using Eq. (3), chemical potential (μ) defined as: $\mu = -\varepsilon_{LUMO} + \varepsilon_{HOMO}/2$, electrophilicity index (ω) using Eq. (4) are obtained for all the rotated conformations.

The global interactions between the compounds of AHH receptors and NA bases have been determined using the parameter charge (ΔN) transferred from a system A to system B, and are represented by [47]:

$$\Delta N = (\mu_{B-\mu_A})/2(\eta_A + \eta_B). \quad (5)$$

The statically thermodynamic functions such as entropy $\left(S_m^0\right)$, enthalpy $\left(H_m^0\right)$ and heat capacity $\left(C_{p,m}^0\right)$ ary depending on the temperature. These thermodynamics parameters of the 4NPA were obtained based on the vibrational analysis at DFT/CAM-B3LYP/6-311++G(*d*,*p*) level.

3.2. Antiproliferative Effect of 4NPA on HeLa Cell Line

The total number of 5×10^4 HeLa cells were seeded in 96-well plates. To determine cell viability, cell proliferation assay (Biological Industries) was used according to the manufacturer's protocol that was described for HeLa cells. For assessing cell viability, HeLa cells were treated with different concentrations of 4NPA for 24 h. Fifty microliters of XTT solution ((2,3-Bis(2-Methoxy-4-Nitro-5-Sulfophenyl)-2H-Tetrazolium-5-Carboxanilide) and activation reagent were added to each well. 96-well plates were incubated at 37°C for 4 h. Formazan product in the supernatant was measured at 480 nm with 96-well plate reader (BIOTEK).

4. RESULTS AND DISCUSSION

4.1. Geometric Parameters and Characterization of 4NPA

The optimized molecular geometry obtained at the DFT/CAM-B3LYP/6-311++G(*d*,*p*) level of the 4NPA monomer according to the atomic number scheme is shown in Fig. 2a. Optimized geometric parameters of this structure are also presented in Table 1. In the benzene ring, the C–C single bond is 1.54 Å and C–N bond is 1.47 Å [48]. In this study, the C–C bond length in the benzene ring ranges between 1.389 and 1.41 Å, C–N bond lengths vary between 1.38 Å and 1.47 Å. The vibrational modes for 4NPA were calculated by DFT method with CAM-B3LYP/6-311++G(*d*,*p*) level of basis set. The 4NPA belonging to C1 point group symmetry and it consists of 22 atoms, which has 60 normal modes of vibrational. The calculated frequencies were scaled with 0.97 [49]. Selected of calculated and experimental Fourier Transform Infrared (FT-IR) frequencies for 4NPA are tabulated in Table 2. The experimental IR spectrum performed with a PerkinElmer Spectrum One FT-IR spectrometer in the range of 4000–450 cm^{-1}. Measured and calculated IR spectrum of the molecule are presented in Figs. 3 and 4, respectively. All these measured bands are seen to match the results compared to the calculated theoretical bands. The most characteristic peaks observed in FT-IR spectrum of 4NPA: C=O amide stretch appears at 1670 cm^{-1} and calculated 1743 cm^{-1} (γ_{str}), this stretching were seen in the region 1600–1715 cm^{-1}

Table 1. Optimized geometrical parameters of 4NPA at DFT/CAM-B3LYP level

Bond	Bond length, Å	Bond	Bond length, Å
C1–C2	1.38	C6–N14	1.40
C1–C6	1.40	N11–O12	1.22
C1–H7	1.08	N11–O13	1.22
C2–C3	1.39	N14–H15	1.01
C2–H8	1.08	N14–C16	1.38
C3–C4	1.38	C16–O17	1.21
C3–N11	1.47	C16–C18	1.49
C4–C5	1.38	C18–H19	1.08
C4–H9	1.08	C18–C20	1.33
C5–C6	1.40	C20–H21	1.08
C5–H10	1.08	C20–H22	1.08
Bond	Bond angle, °	Bond	Bond angle, °
C2–C1–C6	120.78	C4–C5–C6	119.52
C2–C1–H7	119.45	C4–C5–H10	120.68
C6–C1–H7	119.77	C6–C5–H10	119.80
C1–C2–C3	118.71	C1–C6–C5	119.65
C1–C2–H8	121.50	C1–C6–N14	117.08
C3–C2–H8	119.80	C5–C6–N14	123.27
C2–C3–C4	121.52	C3–N11–O12	117.79
C2–C3–N11	119.07	C3–N11–O13	117.65
C4–C3–N11	119.41	O12–N11–O13	124.56
C3–C4–C5	119.82	C6–N14–C16	128.54
C3–C4–H9	119.45	H15–N14–C16	115.92
C5–C4–H9	120.73	N14–C16–O17	123.96
Bond	Bond angle, °	Bond	Bond angle, °
N14–C16–C18	115.39	O17–C16–C18	120.65
Bond	Torsion angle, °	Bond	Torsion angle, °
C6–C1–C2–C3	0.32	C4–C3–N11–O13	179.72
C6–C1–C2–H8	−179.96	C3–C4–C5–C6	0.14
H7–C1–C2–C3	−179.63	C3–C4–C5–H10	179.92
H7–C1–C2–H8	0.08	H9–C4–C5–C6	179.97
C2–C1–C6–C5	−0.33	H9–C4–C5–H10	−0.25
C2–C1–C6–N14	179.82	C4–C5–C6–C1	0.09
H7–C1–C6–C5	179.63	C4–C5–C6–N14	179.93
H7–C1–C6–N14	−0.22	H10–C5–C6–C1	−179.69
C1–C2–C3–C4	−0.09	H10–C5–C6–N14	0.15
C1–C2–C3–N11	179.85	C1–C6–N14–H15	−6.64
H8–C2–C3–C4	−179.81	C1–C6–N14–C16	170.49
H8–C2–C3–N11	0.13	C5–C6–N14–H15	173.52
C2–C3–C4–C5	−0.14	C5–C6–N14–C16	−9.35
C2–C3–C4–H9	−179.97	C6–N14–C16–O17	7.39
N11–C3–C4–C5	179.92	C6–N14–C16–C18	−172.93
N11–C3–C4–H9	0.08	H15–N14–C16–O17	−175.49
C2–C3–N11–O12	179.79	H15–N14–C16–C18	4.19
C2–C3–N11–O13	−0.22	N14–C16–C18–H19	−153.45
C4–C3–N11–O12	−0.27	N14–C16–C18–C20	31.67
O17–C16–C18–H19	26.25	C16–C18–C20–H21	176.44
O17–C16–C18–C20	−148.64	C16–C18–C20–H22	−1.50
H19–C18–C20–H21	1.95		

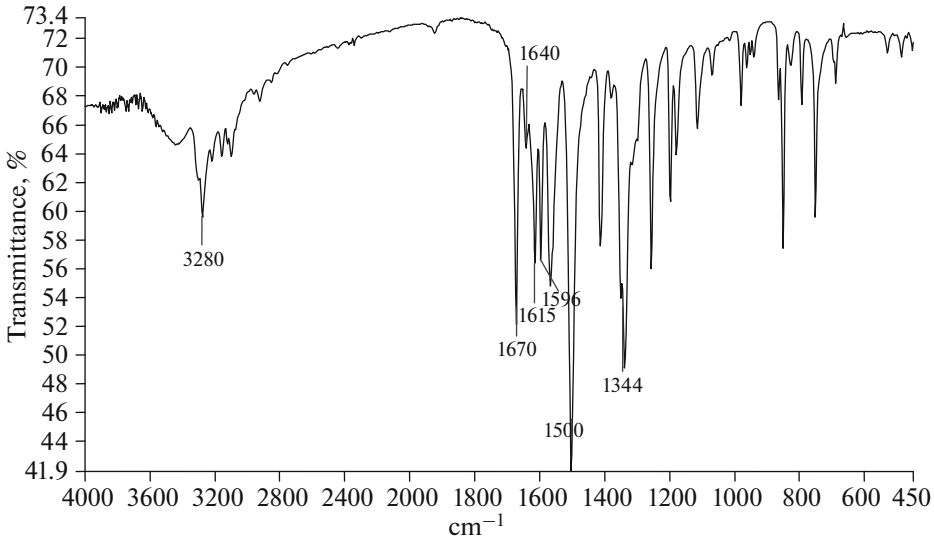

Fig. 3. The experimental FT-IR spectrum of 4NPA.

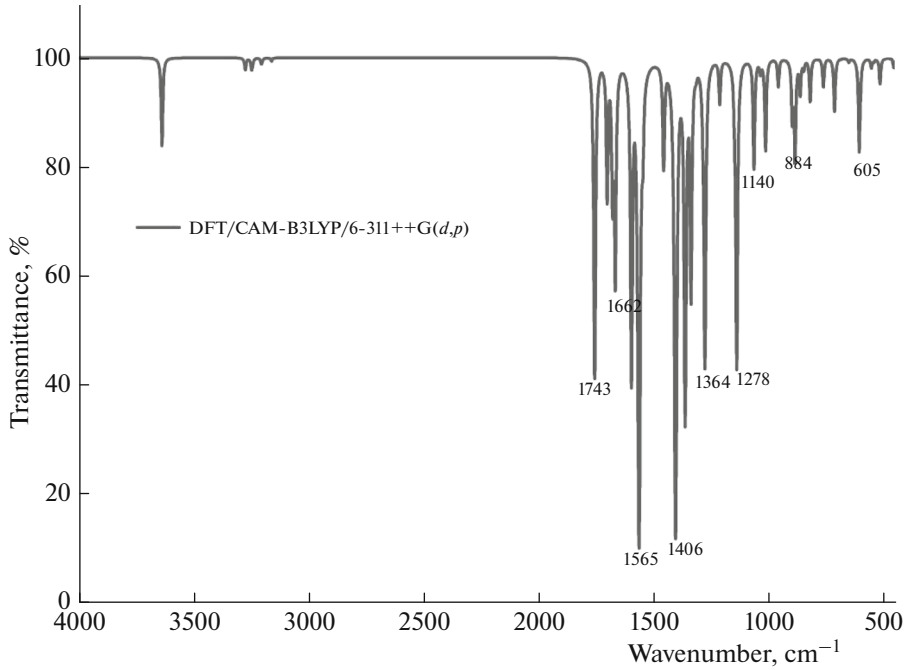

Fig. 4. The calculated (with the scale factor) FT-IR spectrum of 4NPA.

[50, 51], C=C olefinic stretch appears at 1640 and calculated 1662 cm^{-1}, N–H stretch were shown at 3280 cm^{-1} and calculated 3542 cm^{-1}, this stretching vibration observed 3542 cm^{-1} . Same time N–H bending vibration (γ_{bend}) at 1596, C=C stretch on aromatic ring at 1615, asymmetric and symmetric stretch NO_2 ($\gamma_{str\text{-}sym}$) at 1500 and 1344 cm^{-1}.

Experimental Nuclear Magnetic Resonance (NMR) spectra were obtained on a Bruker 400 MHz spectrometer in Dimethyl sulfoxide-d_6 (DMSO-d_6). The theoretical chemical shift values were calculated in DMSO, DMF solvents and gas phase by using The Gauge Independent Atomic Orbital (GIAO) method at CAM-B3LYP/6-311++G(*d*,*p*) level of theory. Tetramethylsilane (TMS) was considered an internal reference. Theoretically calculated ^{13}C-NMR shifts were compared to experimental data before they were scaled with the equation $\delta_{scal} = 0.95\ \delta_{calc} + 0.30$ [52]. The ^{1}H and ^{13}C-NMR spectrums are shown in Figs. 5a, 5b, respectively. The ^{1}H and ^{13}C NMR chemical shift values of the 4NPA are given in Table 3. It is seen that the

Table 2. Comparison of the selected experimental and theoretical vibrational frequencies of 4NPA

Frequencies, cm^{-1}	CAM-B3LYP/6-311++G(*d*,*p*)	Experimental
γ_{str}(C=O)	1743.09	1670
γ_{str} (C=C)	1662.58	1640
γ_{str} (N–H)	3542.44	3280
γ_{bend} (N–H)	1528.72	1596
γ_{str} (C=C) on ring	1625.72	1615
$\gamma_{str\text{-}sym}$ (N–O)	1385.16	1500
$\gamma_{str\text{-}sym}$ (N–O)	1587.89	1344

Table 3. Experimental and calculated chemical shifts (ppm) for 4NPA

Atom	B3LYP/6-311G++(*d*,*p*)			Experimental
	DMSO	DMF	Gas	DMSO
C16	164	164	161	164
C6	146	146	146	147
C3	140	140	140	143
C18	133	133	136	131
C2	126	126	126	125
C4	125	125	124	125
C20	125	125	118	127
C5	115	115	115	125
C1	114	114	112	125
H7	9.1	9.1	9.2	6.5
H9	8.6	8.6	8.6	6.5
H8	8.6	8.6	8.5	6.5
H15	8.0	8.0	7.3	10.8
H10	7.2	7.2	6.7	6.5
H19	6.5	6.5	6.6	6.5
H22	6.4	6.4	5.9	5.9
H21	6.3	6.3	5.9	6.3

chemical shifts in DMF and DMSO solvents are very close to each other and the chemical shifts in the gas phase are the closest to the experimental ones. Also, ^{1}H-NMR spectrum, the following peaks: at 10.8 ppm for N–H, 8.2 and 7.9 ppm aromatic ring protons, 6.5 ppm for =CH olefinic, 6.3 and 5.9 ppm for H_2C=olefinic protons. ^{13}C-NMR spectrum, the following peaks: at 164 ppm for C=O, 147 ppm for C–NH, 143 ppm for C–NO_2, 131 ppm for =CH olefinic, 125 and 119 ppm for aromatic ring carbons, 127 ppm for =CH_2.

4.2. Reactivity Descriptors

The relative energy, electronic spatial coverage values as electronic volume measurement and global chemical reactivity descriptors such as chemical hardness, electronegativity and electrophilicity index of

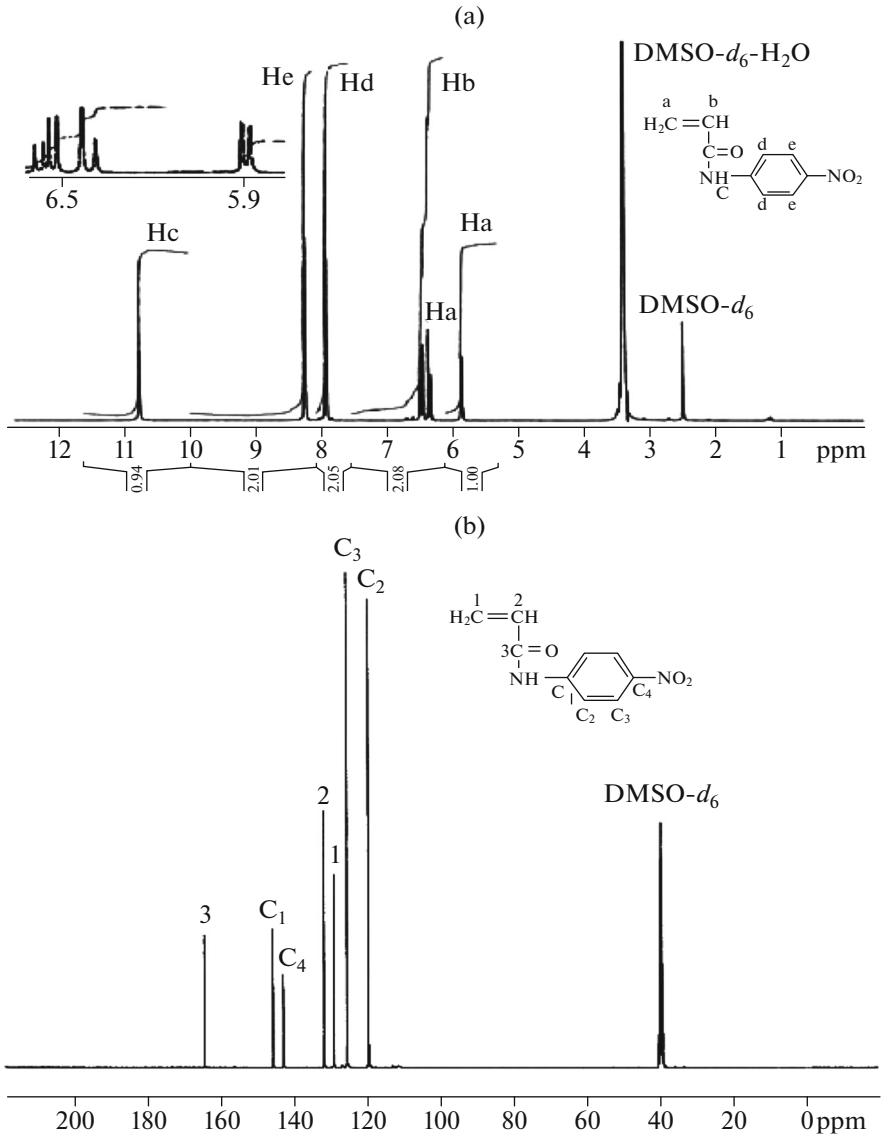

Fig. 5. (a) ^{1}H NMR spectra of 4NPA in DMSO solution; (b) ^{13}C NMR spectra of 4NPA in DMSO solution.

4NPA optimized at CAM-B3LYP/6-311++G(*d*,*p*) for the different torsional angle are calculated and are listed (Table 4). The variation of relative energy of 4NPA are displayed in Fig. 6 for various rotational angles. The most stable conformation corresponds to $\varphi = 180°$ rotated conformation about C–N (16 and 14) bond. The rotational energy barrier is between 0 and 47.154 kJ/mol (Fig. 6). Due to this remarkable energy variation, the molecule is less flexible and this does not allow 4NPA easily interact with the cellular components in the environment in which it resides and hence it has low toxicity. Maximum chemical hardness values coincide with $\varphi = 180°$ and this is also the minimum energy conformation of 4NPA. The minimum hardness value of 4NPA is seen at 90° and 270°, respectively, which are the most unstable conformation (Fig. 6).

The electrophilicity index, a measure of the ability to gain additional electronic charge around the electron acceptors, is important in terms of providing useful information about the active sites of the electrophiles. The plot of global electrophilicity index (ω) with torsional angle (Fig. 7) shows high electrophilicity value for the conformations $\varphi = 0°$ and $\varphi = 360°$. It is clear that the electrophilicity profile that $\varphi = 0°$ and $\varphi = 360°$ conformations are also high for the ω. In addition, according to Parr et al. [53], the most stable conformation of a molecule must have the lowest electrophilicity index. This situation is clearly seen in Fig. 7. Figure 8 shows the change in electronegativity and torsional angle, which has a half value of the energy gap between HOMO and LUMO. The smaller this value is for the molecule, the more toxic the molecule can be. It can be said that the 4NPA molecule has the lowest

Table 4. Calculated relative energy, electronic spatial extent, chemical hardness, electronegativity, electrophilicity index of 4NPA

Torsion angle[a]	Relative energy[b]	Electronic spatial extent[c]	Chemical hardness[d]	Electronegativity[d]	Electrophilicity index[d]
0	24.22	3869.20	3.30	5.19	4.08
30	25.91	3865.71	3.24	5.10	4.02
60	42.02	3834.96	3.18	4.99	3.92
90	47.15	3811.37	3.18	4.94	3.84
120	23.85	3783.32	3.23	5.06	3.96
150	4.63	3822.16	3.24	5.10	4.01
180	0.00	3862.92	3.34	5.04	3.80
210	4.63	3864.79	3.24	5.10	4.01
240	23.85	3823.18	3.23	5.06	3.96
270	47.15	3792.81	3.18	4.94	3.84
300	42.02	3805.77	3.18	4.99	3.92
330	25.91	3835.50	3.24	5.10	4.02
360	24.22	3864.97	3.31	5.19	4.08

[a] In degrees.
[b] In kJ/mol.
[c] In a.u.
[d] In eV.

electronegativity and the greatest toxicity values at 90° and 270° conformation.

Table 5 reports the total electronic energy (E) and global reactivity descriptors (χ, η, and μ for nucleic acid bases *viz.*, Adenine, Guanine, Cytosine, Thymine, Uracil and for Phenyalanine and Histidine from AHH receptors. There is always electron flows from less electronegative system to more electronegative system [34]. Charge transfer calculation for detecting electron transfer between 4NPA and bases, AHH receptors are reported showing clearly the electron donating nature of 4NPA. To quantitatively estimate the electron transfer in the interaction of nucleic acid bases and AHH receptors with 4NPA, we have calculated the amount of charge transfer between 4NPA and model biomolecules by applying Eq. (5). It is seen

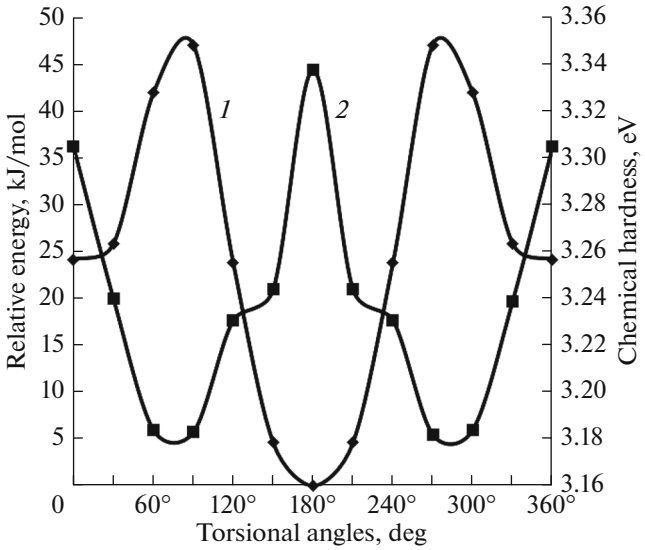

Fig. 6. Variation of the relative energy and chemical hardness (eV) with the torsional angles of 4NPA: (*1*) relative energy, kJ/mol; (*2*) chemical hardness, eV.

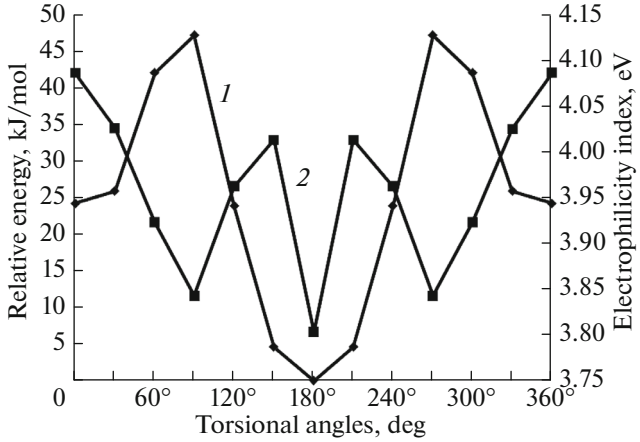

Fig. 7. The variation of the relative energy and global electrophilicity index with the torsional angles of 4NPA: (*1*) relative energy, kJ/mol; (*2*) electrophilicity index, eV.

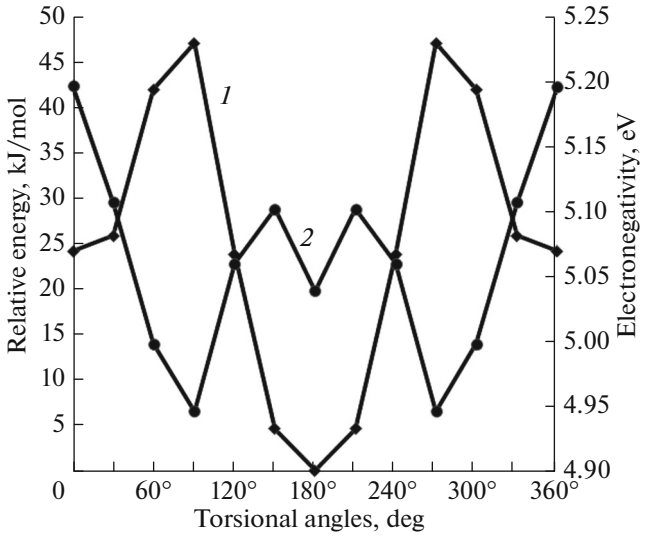

Fig. 8. The variation of Electronegativity with the torsional angles of 4NPA: (*1*) relative energy, kJ/mol; (*2*) electronegativity, eV.

that all ΔN values are positive and thus 4NPA acts as an electron acceptor in its reactions with its receptors. Hence, these nucleic acid bases and AHH receptors can be characterized as electron donors interacting with 4NPA (Fig. 9). This can also be explained as follows: all nucleic acid bases have a chemical potential of less than 4 NPA molecule. Thus, when the 4NPA molecule interacts with model biomolecules, electrons flow from the less electronegative nucleic acid bases and AHH receptors towards the 4NPA molecule. The electron transfer for all the model biomolecules have a minimum value for the φ = 270° configuration and maximum value for the φ = 0° and 360° (Fig. 9). It also may be noted from Fig. 9, 4NPA interacts with these model biomolecules, while guanine and histidine donate the maximum charge, respectively, while adenine and uracil donate the minimum charge. Frontier molecular orbitals were calculated at the same level of theory. The 3D diagram for the four most important molecular orbitals named HOMO, LUMO, HOMO-1 and LUMO+1 in the most stable state of the head molecule is shown in Fig. 10. It shows that the HOMO and LUMO orbitals are localized on almost all of the molecule. Also, red color indicates the presence of electrons or negative charges, and the green color indicates the absence of electrons or positive charges. For 4NPA, HOMO orbital energy was calculated as –8.359 eV, HOMO-1 level –9.321 eV, LUMO level –1.866 eV and LUMO+1 level –0.455 eV. The HOMO-LUMO energy gap was estimated at 6.492 eV at the DFT/CAM-B3LYP level. This high HOMO-LUMO energy gap means good stability, low reactivity and low toxicity for 4NPA monomer.

Table 5. Calculated chemical hardness and chemical potential of the NA bases and AHH receptors

Bases and receptors	Electronic energy, eV	Electronegativity, eV	Chemical hardness, eV	Chemical potential, eV
Adenine	–12714.147	4.50	3.96	–4.50
Thymine	–12356.102	4.17	4.12	–4.17
Guanine	–14762.333	3.59	4.03	–3.59
Cytosine	–10744.468	4.08	3.74	–4.08
Histidine	–14930.547	3.76	4.08	–3.76
Uracil	–11286.560	4.39	4.25	–4.39
Phenylalanine	–15093.754	4.02	4.40	–4.02

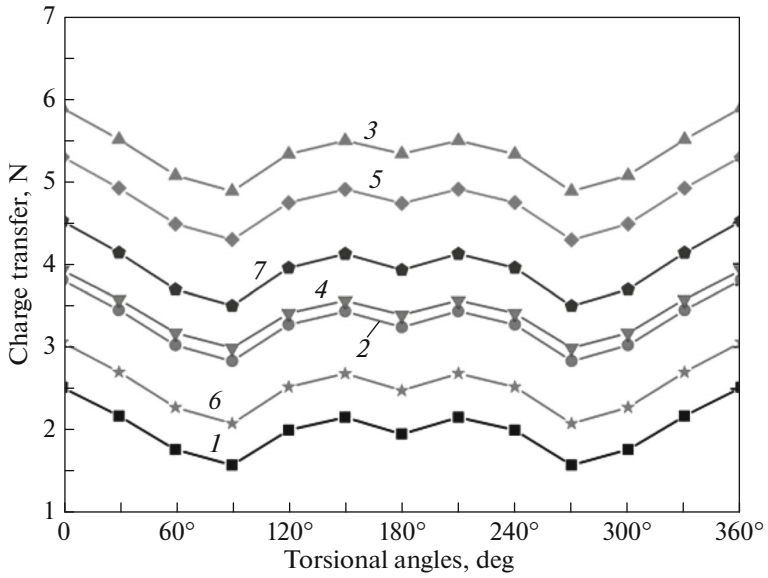

Fig. 9. Charge Transfer between 4NPA with various torsional angles NA bases and AHH receptors: (*1*) adenine; (*2*) thymine; (*3*) guanin; (*4*) cytosine; (*5*) histidine; (*6*) uracil; (*7*) phenylalanine.

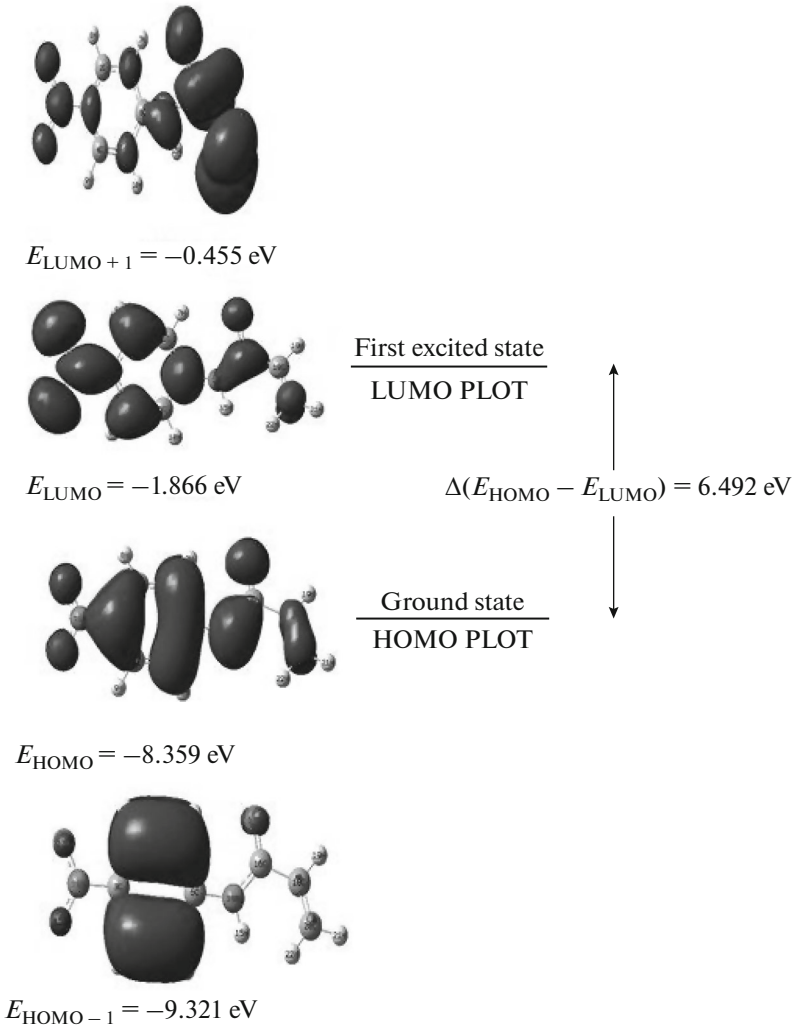

Fig. 10. The frontier molecular orbitals of 4NPA for gas phase.

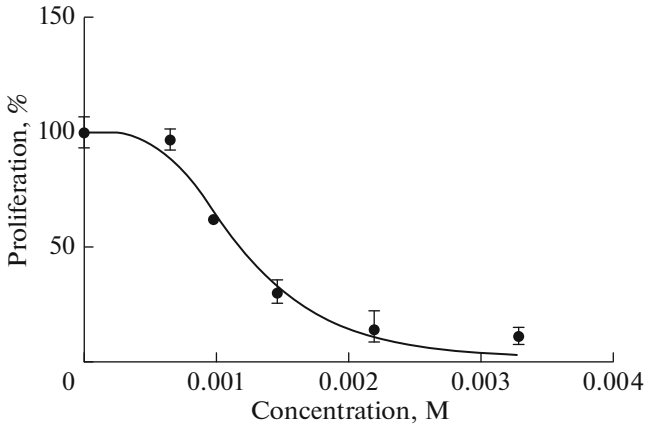

Fig. 11. Cytotoxicity analyses of 4NPA on HeLa cells.

5. ANTIPROLIFERATIVE ACTIVITY

Cell proliferation assay was performed by using XTT reagent to determine the effects of 4NPA on HeLa cells. XTT results demonstrate the antiproliferative effect of 4NPA on HeLa cells. The determined half maximal inhibitory concentration (IC50) value for HeLa cells were 1mM by 4NPA (see Fig. 11).

6. CONCLUSIONS

In this study, *N*-(4-nitrophenyl)acrylamide (4NPA) compound was synthesized and characterized by FT-IR, ^{1}H and ^{13}C-NMR spectroscopy techniques. Both experimental and theoretical methods showed that the compound was successfully synthesized. The results showed that the calculated frequencies and chemical shifts correspond to the experimental values. Both experimental (antiproliferative activity) and theoretically (DFT-based reactivity descriptors) we have seen that 4 NPA molecule has low toxicity. In addition, theoretically calculated low HOMO-LUMO energy range supports low toxicity of the molecule. Selected nucleic acid bases and AHH receptors have a chemical potential of less than 4NPA molecule. Thus, when interacting with nucleic acid bases and AHH receptors, electrons will flow to less electronegative nucleic acid base than to electronegative 4NPA molecule. In other words, the 4NPA molecule acts as an electron acceptor when it interacts with a biosystem such as phenylalanine and histidine from NA bases and AHH receptors.

ACKNOWLEDGMENTS

The numerical calculations were performed at TUBITAK ULAKBIM, High Performance and Grid Computing Center and Ahi Evran University, Research and Application Center. We are thankful to TUBITAK and Kırşehir Ahi Evran University.

REFERENCES

1. R. Baskaya, Y. Keskin, A. Karagoz, and H. I. Koc, Prevent. Med. Bull. **8**, 2 (2009).
2. E. Dybing and T. Sanner, Toxicol. Sci. **75**, 1 (2003).
3. http://fao.org/tempref/codex/Meetings/CCASIA/CCASIA13/as0209ae.pdf/2002.
4. http://who.int/foodsafety/fs_management/No_02_Acrylamide_Mar05_en_rev1.pdf.
5. A. Becalski, B. P. Lau, D. Lewis, and S. W. Seaman, in *Proceedings of the AOAC Annual Meeting and Exposition, Los Angeles, CA, 2002,* p. 22.
6. P. Rydberg, S. Ericson, E. Tareke, et al., J. Agric. Food Chem. **5**, 7012 (2003).
7. R. H. Stadler, I. Blank, N. Varga, et al., Nature (London, U.K.) **419**, 449 (2002).
8. C. Ruden, Food Chem. Toxicol. **42**, 3 (2004).
9. http://www.who.int/foodsafety/areas_work/chemical-risks/acrylamide/.
10. K. M. Marstokk, H. Møllendal, and S. Samdal, J. Mol. Struct. **524**, 1 (2000).
11. A. K. Chandra and M. T. Nguyen, J. Phys. Chem. A **102**, 30 (1998).
12. S. Arulmozhiraja, T. Fujii, and G. Sato, Mol. Phys. **100**, 4 (2002).
13. S. Arulmozhiraja, P. C. Selvin, and T. Fujii, J. Phys. Chem. A **106**, 9 (2002).
14. M. Nendza, J. Volmer, and W. Klein, *Practical Applications of Quantitative Structure-Activity Relationships (QSAR) in Environmental Chemistry and Toxicology* (Kluwer, Dordrecht, Netherlands, 1990).
15. T. W. Schultz, Toxicol. Methods **7**, 289 (1997).
16. S. D. Dimitrov, O. G. Mekenyan, and T. W. Schultz, Bull. Environ. Contam. Toxicol. **65**, 399 (2000).
17. P. K. Chattaraj, S. Nath, and B. Maiti, *Computational Medicinal Chemistry for Drug Discovery* (Marcel Dekker, New York, 2003).
18. R. Parthasarathi, J. Padmanabhan, V. Subramanian, B. Maiti, and P. K. Chattaraj, J. Phys. Chem. A **107**, 13046 (2003).
19. R. Parthasarathi, J. Padmanabhan, V. Subramanian, B. Maiti, and P. K. Chattaraj, Curr. Sci. **86**, 535 (2004).

20. J. Padmanabhan, R. Parthasarathi, U. Sarkar, V. Subramanian, and P. K. Chattaraj, Chem. Phys. Lett. **383**, 1 (2004).
21. R. K. Roy, F. de Proft, and P. Geerlings, J. Phys. Chem. A **102**, 7035 (1998).
22. F. Mendez, J. Tamariz, and P. Geerlings, J. Phys. Chem. A **102**, 6292 (1998).
23. W. Langenaeker, F. de Proft and P. Geerlings, J. Phys. Chem. A **102**, 5944 (1998).
24. R. K. Roy, S. Krishnamurthy, P. Geerlings, and S. Pal, J. Phys. Chem. A **102**, 3746 (1998).
25. A. Chatterjee, T. Iwasaki, and T. Ebina, J. Phys. Chem. A **103**, 2489 (1999).
26. P. Perez, A. Toro-Labbe, and R. Contreras, J. Phys. Chem. A **103**, 11246 (1999).
27. P. Jaque and A. Toro-Labbe, J. Phys. Chem. A **104**, 995 (2000).
28. P. Perez, A. Toro-Labbe, and R. Contreras, J. Phys. Chem. A **104**, 5882 (2000).
29. S. Gutierrez-Oliva, P. Jaque, and A. Toro-Labbe, J. Phys. Chem. A **104**, 8955 (2000).
30. G. Schuurmann, Environ. Toxicol. Chem. **9**, 417 (1990).
31. S. Kobayashi, K. Sameshima, Y. Ishii, and A. Tanaka, Chem. Pharm. Bull. **43**, 1780 (1995).
32. R. G. Parr and W. Yang, Ann. Rev. Phys. Chem. **46**, 701 (1995).
33. H. Chermette, J. Comput. Chem. **20**, 129 (1999).
34. R. Parthasarathi, J. Padmanabhan, U. Sarkar, et al., El. J. Mol. Des. **2**, 798 (2003).
35. D. R. Roy, R. Parthasarathi, B. Maiti, V. Subramanian, and P. K. Chattaraj, Bioorg. Med. Chem. **13**, 3405 (2005).
36. N. Cankaya and M. M Temuz, Cellulose Chem. Technol. **46**, 9 (2012).
37. M. J. Frisch et al., *Gaussian 09, Revision A.1* (Gaussian, Inc., Wallingford, CT, 2009).
38. Y. Tawada, T. Tsuneda, S. Yanagisawa, et al., J. Chem. Phys. **120**, 8425 (2004).
39. T. Yanai, P. D. Tew, and C. N. Handy, Chem. Phys. Lett. **393**, 51 (2004).
40. M. J. G. Peach, E. I. Tellgren, P. Salek, et al., J. Phys. Chem. A **111**, 11930 (2007).
41. A. L. Peter, V. M. Kurt, and P. L. Hans, J. Chem. Phys. **130**, 194114 (2009).
42. K. Fukui, Science (Washington, DC, U. S.) **218**, 747 (1987).
43. R. G. Parr and W. Yang, *Density-Functional Theory of Atoms and Molecules* (Oxford Univ. Press, New York, 1989).
44. R. G. Pearson, *Chemical Hardness—Applications from Molecules to Solids* (VCH-Wiley, Weinheim, 1997).
45. R. P. Iczkowski and J. L. Margrave, J. Am. Chem. Soc. **83**, 3547 (1961).
46. R. G. Parr, L. V. Szentpaly, and S. J. Liu, Am. Chem. Soc. **121**, 1922 (1999).
47. R. G. Parr and R. G. Pearson, J. Am. Chem. Soc. **105**, 7512 (1983).
48. J. J. Nie and D. J. Xu, Chin. Struct. J. Chem. **21**, 165 (2002).
49. D. C. Young, *Computational Chemistry* (Wiley, New York, 2001).
50. M. Barthes, G. de Nunzio, and M. Ribet, Synth. Met. 76, 1, (1996).
51. N. P. G. Roeges, *A Guide to the Complete Interpretation of IR Spectra of Organic Compounds* (Wiley, New York, 1994).
52. A. E. Aliev, D. Courtier-Murias, and S. Zhou, J. Mol. Struct.: THEOCHEM **893**, 1 (2009).
53. R. G. Parr and W. Yang, J. Am. Chem. Soc. **106**, 4049 (1984).